Title

A bio-instructive parylene-based conformal coating suppresses thrombosis and intimal hyperplasia of implantable vascular devices

Authors

Hao, Dake

Lin, Jonathan

Liu, Ruiwu

et al.

Publication Date

2023-10-01

DOI

10.1016/j.bioactmat.2023.06.014

Peer reviewed

Bioactive Materials 28 (2023) 467–479

Contents lists available at ScienceDirect

Bioactive Materials

journal homepage: www.keaipublishing.com/en/journals/bioactive-materials

A bio-instructive parylene-based conformal coating suppresses thrombosis and intimal hyperplasia of implantable vascular devices

Dake Hao [a,b], Jonathan Lin [a], Ruiwu Liu [c], Christopher Pivetti [a,b], Kaeli Yamashiro [a], Linda M. Schutzman [a], Junichiro Sageshima [a], Mimmie Kwong [a], Nataliya Bahatyrevich [a], Diana L. Farmer [a,b], Misty D. Humphries [a], Kit S. Lam [c], Alyssa Panitch [d,e], Aijun Wang [a,b,e,*]

[a] Department of Surgery, School of Medicine, University of California Davis, Sacramento, CA, 95817, United States
[b] Institute for Pediatric Regenerative Medicine, Shriners Hospitals for Children, Sacramento, CA, 95817, United States
[c] Department of Biochemistry and Molecular Medicine, School of Medicine, University of California Davis, Sacramento, CA, 95817, United States
[d] Wallace H. Coulter Department of Biomedical Engineering, Georgia Institute of Technology and Emory University, Atlanta, GA, 30332, United States
[e] Department of Biomedical Engineering, University of California Davis, Davis, CA, 95616, United States

ARTICLE INFO

Keywords:
Parylene coating
Integrin ligand
Thrombosis
Intimal hyperplasia
Implantable vascular devices

ABSTRACT

Implantable vascular devices are widely used in clinical treatments for various vascular diseases. However, current approved clinical implantable vascular devices generally have high failure rates primarily due to their surface lacking inherent functional endothelium. Here, inspired by the pathological mechanisms of vascular device failure and physiological functions of native endothelium, we developed a new generation of bioactive parylene (poly(p-xylylene))-based conformal coating to address these challenges of the vascular devices. This coating used a polyethylene glycol (PEG) linker to introduce an endothelial progenitor cell (EPC) specific binding ligand LXW7 (cGRGDdvc) onto the vascular devices for preventing platelet adhesion and selectively capturing endogenous EPCs. Also, we confirmed the long-term stability and function of this coating in human serum. Using two vascular disease-related large animal models, a porcine carotid artery interposition model and a porcine carotid artery-jugular vein arteriovenous graft model, we demonstrated that this coating enabled rapid generation of self-renewable "living" endothelium on the blood contacting surface of the expanded polytetrafluoroethylene (ePTFE) grafts after implantation. We expect this easy-to-apply conformal coating will present a promising avenue to engineer surface properties of "off-the-shelf" implantable vascular devices for long-lasting performance in the clinical settings.

1. Introduction

As the incidence of vascular diseases continues to rise worldwide, there is a corresponding increase in the demand for treatment interventions, most of which require various implantable vascular devices [1]. Implantable vascular devices are currently widely used in clinical settings because they are relatively easy to apply and available off-the-shelf. However, they also have high failure rates due to thrombosis and intimal hyperplasia [2–5]. To address these challenges of the implantable vascular devices, it is advisable to engineer the surface of the vascular devices directly targeting the pathological mechanisms and process of vascular device failure and mimicking the physiological functions of native endothelium. Platelet activation, aggregation and adhesion on the surface of the devices can happen quickly after the implantation of "foreign" vascular devices, which is the crucial cause for thrombosis [6,7]. Moreover, the native functional endothelium produces hemostatic regulatory molecules and displays a variety of characteristics, such as anti-platelet adhesion, anti-inflammatory responses, and modulation of vascular tone, that are important to maintain normal vascular functions and suppress intimal hyperplasia [8–12]. However, most prosthetic vascular devices possess no regenerative potential and one of the major causes of their failure rate is the lack of a functional endothelium [13–15]. Thus, establishment of an engineered surface on the implantable vascular devices that could suppress platelet adhesion

Peer review under responsibility of KeAi Communications Co., Ltd.
* Corresponding author. Center for Surgical Bioengineering, Department of Surgery, School of Medicine, University of California, Davis, 4625 2nd Ave., Research II, Suite 3005, Sacramento, CA, 95817, United States.
E-mail address: aawang@ucdavis.edu (A. Wang).

https://doi.org/10.1016/j.bioactmat.2023.06.014
Received 5 April 2023; Received in revised form 17 June 2023; Accepted 19 June 2023

and simultaneously promote rapid endothelialization to develop a healthy endothelium, holds the promise for preventing the implanted vascular devices from thrombosis and intimal hyperplasia.

Currently, the approach of greatest interest for achieving rapid endothelialization on the surface of implantable vascular devices is to facilitate the adhesion of circulating endogenous endothelial progenitor cells (EPCs) and endothelial cells (ECs) [16–21]. During the process of tissue regeneration, integrins play the critical role in anchoring cells to the extracellular matrix (ECM) and regulating intracellular signals [22–27]. The utilization of ECM-derived functional sequences, such as the arginine-glycine-aspartic acid (RGD) peptide, to promote endothelialization of vascular devices has also been investigated [28]. Although the ECM-derived ligand RGD has shown capability of promoting EPC and EC binding [29], it also presented strong binding to platelets via integrin αIIbβ3 that is the main factor mediating platelet adhesion [30,31]. To develop the integrin-based specific EPC/EC binding ligand, we used One-Bead One-Compound (OBOC) high-throughput combinatorial screening technology and identified a ligand LXW7 which possesses high binding affinity to integrin αvβ3 but very low binding affinity to integrin αIIbβ3 [32]. We have demonstrated LXW7 showed stronger binding affinity to human EPCs and ECs derived from different tissue sources and species, but extremely weaker binding to platelets, compared with the conventional RGD peptide [32–37], indicating LXW7's potential application in supporting specific EPC/EC binding. Furthermore, polyethylene glycol (PEG), a FDA-approved non-toxic, non-immunogenic, non-antigenic synthetic polymer [38], has been used for surface modification of materials to prevent platelet adhesion [39,40]. PEG also can be used as a multifunctional linker to facilitate covalent conjugation of functional molecules to the device surface [41,42].

In addition, most of the current "clinical-grade" implantable vascular devices are chemically and biologically inert [43–45], which also makes stable and uniform surface modification of these materials technically challenging. Parylene, a variety of poly(p-xylylene) polymers, have been widely used as moisture and dielectric barriers to uniformly coat implantable medical devices due to their excellent mechanical flexibility and long-lasting *in vivo* adherence to the device surface [46–50]. Parylene can be conformally coated onto irregular substrates by a chemical vapor deposition (CVD) process and are chemically stable, nonbiodegradable, and essentially substrate independent. The FDA has approved parylene as Class VI polymers for coating medical devices [51]. In this study, we developed a new generation of bioactive parylene-based conformal coating with a PEG linker to present LXW7 to simultaneously suppress platelet adhesion at the acute stage, promote EPC binding at the early stage, and support rapid endothelialization at the late stage on the surface of implantable vascular devices to prevent thrombosis and neointimal hyperplasia. The overall strategy of this conformal coating was shown in Fig. 1A. We demonstrated that this conformal coating significantly inhibited platelet adhesion and improved EPC adhesion and proliferation on the surfaces of expanded polytetrafluoroethylene (ePTFE) vascular grafts, bare-metal stents, and valves. We further evaluated the function of the ePTFE grafts with this conformal coating in two vascular disease-related large animal models, a porcine carotid artery interposition model and a porcine carotid artery-jugular vein arteriovenous graft model and confirmed this conformal coating effectively enabled rapid generation of self-renewable "living" endothelium, suppressed thrombosis and intimal hyperplasia, and improved patency of ePTFE grafts.

2. Materials and methods

2.1. Cell culture and platelet isolation

Human endothelial colony forming cells (ECFCs) were isolated from human umbilical cord blood as previously described [32–34]. The ECFCs were expanded and cultured in Endothelial Growth Medium-2 (EGM-2, Lonza). ECFCs between P3 and P6 were used for all experiments. For platelet isolation, whole blood was collected from healthy human volunteers with informed consent by venipuncture following the approved UC Davis IRB protocol. Approximately 20 ml blood was collected into citrated glass vacutainers (BD Bioscience). The blood was then centrifuged for 20 min at 200×*g* at 25 °C to obtain platelet rich plasma (PRP), which is the top layer of the centrifuged blood.

2.2. Parylene-PEG-LXW7 coating

Parylene-PEG-LXW7 was successfully coated onto the ePTFE grafts with 6 mm inner diameter (Gore-Tex), bare-metal stents and valves (Medtronic Inc.) by the following steps. Firstly, parylene-A (Angene International Limited) was coated on the ePTFE grafts, stents and valves via a chemical vapor deposition (CVD) process in a PDS 2010 coater (SCS Specialty Coating Systems) as the previously described [52,53]. Briefly, the dimeric Parylene-A powder was sublimated to gas at 160 °C; pyrolised to form the gaseous monomer at 650 °C; and finally deposited on the graft surface as a polymer film at 25 °C. The uniformity of parylene-A coating was characterized by using ninhydrin analysis method that was employed to quantitatively detect amino groups. Briefly, the parylene-A coated ePTFE graft was immersed in 1.0 mol/L ninhydrin/ethanol solution for 1 min and followed by heating at 75 °C for 15 min in a water bath to accelerate the reaction between ninhydrin and amino groups. Coating thicknesses of parylene-A was measured on a simultaneously coated Si wafer by using a SE 801 spectroscopic ellipsometer and a Dektak 3030 Surface Profilometer. Secondly, the azido-PEG12-NHS ester (BroadPharm) was covalently conjugated to the amino groups on the parylene-A. Lastly, the LXW7-DBCO (Fig. S1) was then conjugated to the azido groups via Cu-free click chemistry. The surface elemental composition was verified by using an Axis Nova x-ray photoelectron spectroscopy (XPS) system (Kratos Analytical) with monochromatic Al Kα X-Ray source. Amino Acid Analysis (AAA) was used to quantify the amount of LXW7 bonded onto the grafts. Samples were hydrolyzed by a solution of 6 M HCl with 1% of phenol at 110 °C for 24 h under vacuum into individual amino-acid residues. The individual amino acids were separated by ion-exchange chromatography, postcolumn derivatized by ninhydrin and measured by a Beckman 6300 amino-acid analyzer (Beckman).

2.3. Cytotoxicity test

2×10^5 ECFCs with EGM-2 were seeded in the lower chamber of the transwell system (24-well plate, 8 μm, Corning) with or without PPL-ePTFE graft placed in the upper chamber. After incubating for 24 h, the viability of ECFCs was determined by using LIVE/DEAD® Viability/Cytotoxicity Kit (Molecular Probes). Stained constructs were imaged using the Zeiss Observer Z1 microscope, and images further processed with ImageJ software.

2.4. Tensile strength measurement

The ePTFE grafts with different coatings were tested under tension at a rate of 5%/min on a mechanical testing apparatus (Instron) with a 1000 N load cell until failure [54]. Ultimate tensile strength (UTS) was calculated from the load vs extension data based on initial sample geometries. UTS was determined as the maximum stress of each sample's stress strain curve.

2.5. Contact angle measurement

The captive bubble technique was used for contact angle measurement because the surfaces are constantly in contact with fluid media. The captive bubble contact angle measurements were taken at 22 °C using a video capture system (OCA 40, Data Physics Instruments GmbH, Filderstadt, Germany). One drop of water was dripped on the graft

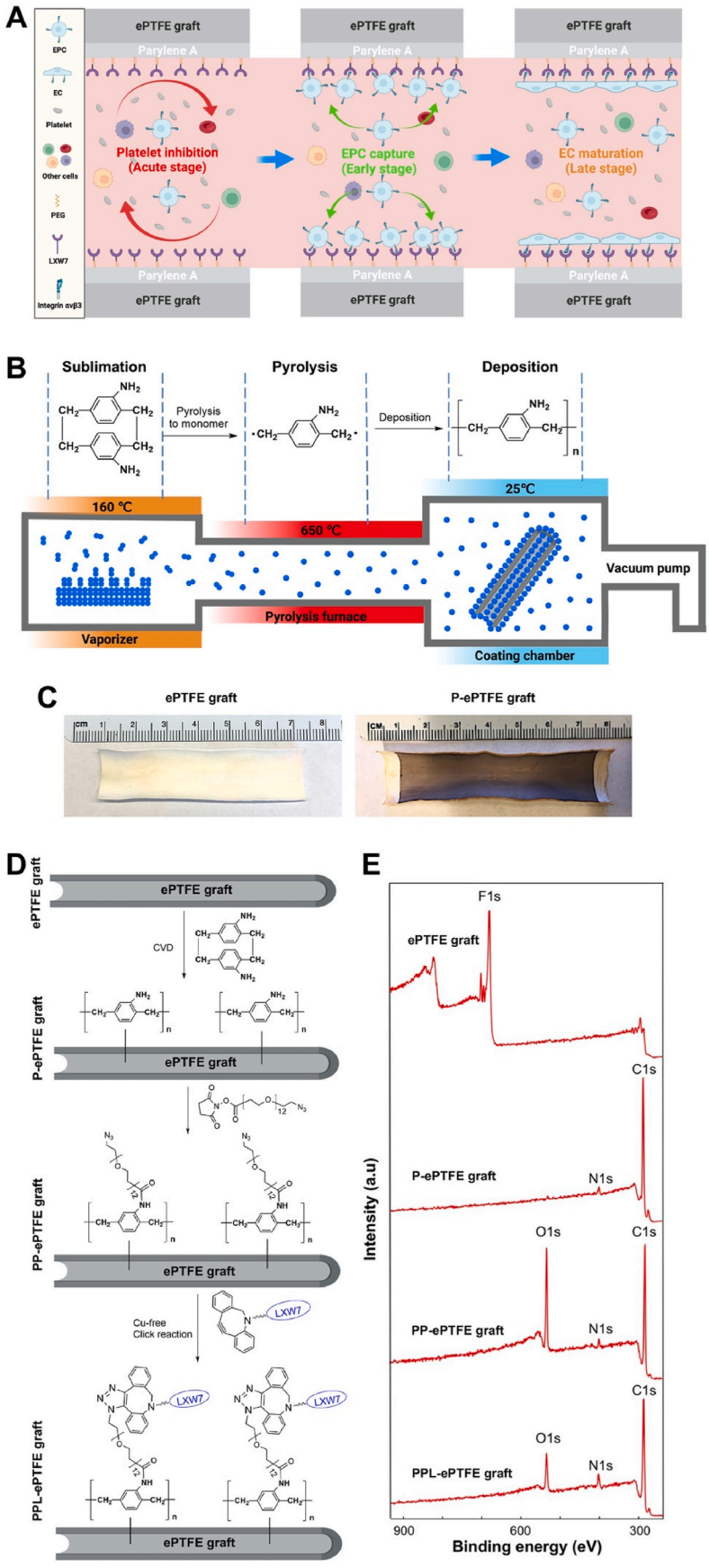

Fig. 1. Construction and characterization of PPL-ePTFE grafts. (A) The overall schematic diagram showing the mechanism of action of the PPL-ePTFE grafts. (B) The general process of parylene-A coating using CVD which involves three major steps: sublimation in vaporizer, pyrolysis in paralysis furnace, and deposition in the coating chamber. (C) Ninhydrin reaction on the P-ePTFE grafts, confirming the presence of conformal primary amine groups on the surface of the ePTFE grafts after parylene-A coating. (D) The step-by-step process of the construction of PPL-ePTFE grafts. (E) XPS characterization of ePTFE grafts, P-ePTFE grafts, PP-ePTFE grafts, and PPL-ePTFE grafts. Nitrogen was identified on the P-ePTFE grafts, PP-ePTFE grafts, and the PPL-ePTFE grafts, but not on the ePTFE grafts.

surfaces. After a few seconds, the static contact angle near the three-phase line was measured.

2.6. Platelet adhesion and activation

Fresh PRP was seeded on the surface of ePTFE grafts, stents, and valves for 1 h at 37 °C. After 1 h of incubation, the PRP was removed, and the grafts, stents and valves were washed 3 times with PBS (Gibco), stained with Calcein-AM (Thermo Fisher Scientific). Samples were analyzed using a Zeiss Observer Z1 microscope. Quantification of images was performed using the ImageJ software (NIH). The platelets adhered on the grafts were determined by using a scanning electron microscopy (SEM, Quattro, Thermo Fisher Scientific).

2.7. ECFC adhesion and proliferation

ECFCs in EGM-2 medium were seeded on the ePTFE grafts, stents, and valves with different coatings at a density of 1×10^4 cells/cm^2. For the cell adhesion test, after 0.5 h of incubation, the medium was aspirated, unattached cells were washed off 3 times with PBS. The adhered cells were stained with Calcein-AM and characterized using the Zeiss Observer Z1 microscope. The number of the adhered cells was quantified using ImageJ software. For the cell proliferation test, after 1 h of incubation, new additional EGM-2 medium was added into the dishes, and the cells were subsequently cultured for 7 d. The cell viability was determined by using MTS assay (Promega) according to the instructions at day 1 and day 7. The amount of soluble formazan product produced by the reduction of MTS by metabolically active cells was measured at the 490 nm absorbance using the SpectraMax i3x Multi-Mode Detection Platform.

2.8. Serum stability

Parylene-PEG-LXW7 coated ePTFE grafts were incubated in human serum (Millipore) for 100 days at 37 °C. Serum was changed twice per week. At different time points, the parylene-PEG-LXW7 coated ePTFE grafts were taken out from the serum and washed with PBS 3 times, and the human ECFC adhesion assay was performed for the grafts. The number of cells adhered on the grafts was determined by using MTS assay.

2.9. Activated partial thromboplastin time

Blood was obtained from healthy volunteers by vena puncture and mixed with sodium citrate (0.3% final concentration). After centrifuging at 3500 rpm for 12 min, the supernatant (platelet poor plasma, PPP) was used for the following experiments. Activated partial thromboplastin time (APTT) is a simple and highly reliable measurement of the capacity of blood to coagulate through the intrinsic coagulation mechanism and the effect of the biomaterial on possible delay of the process. 100 μl PPP was pre-incubated with the ePTFE, P-ePTFE, PP-ePTFE or PPL-ePTFE grafts at 37 °C, then activated by addition of rabbit brain cephalin (Sigma). The samples were incubated at 37 °C for 5 min and then incubated with calcium chloride. Immediately, the time for initiation of clot formation, detected by using a steel hook.

2.10. Prothrombin time

Prothrombin time (PT) was measured to assess hylan-induced deferment or interdiction of the extrinsic coagulation pathway. 100 μl PPP was layered atop the ePTFE, P-ePTFE, PP-ePTFE or PPL-ePTFE grafts at 37 °C and supplemented with thromboplastin (Factor III, Sigma) containing Ca^{2+} was added to the PPP. The time taken for the onset of fibrin (clot) formation was detected using a steel hook.

2.11. Hemolysis test

Red blood cell (RBC) dispersions (the precipitation after whole blood centrifuge at 3000 rpm/min for 15 min) were incubated with ePTFE, P-ePTFE, PP-ePTFE or PPL-ePTFE grafts respectively at 37 °C for 1 h, then centrifuged at 2000 rpm/min for 5 min. A 100 mL aliquot of supernatant was taken for measurement at 545 nm using a microplate reader (EPOCH2, BioTek, Winooski, VT, USA). The hemolysis ratio (%) = DF-DP/DN-DP × 100. In this equation, DF, DN, and DP are the absorbance at 545 nm of the graft sample, distilled water (negative control), and saline (positive control), respectively.

2.12. Porcine carotid artery interposition model

All animal procedures were approved by the Institutional Animal Care and Use Committee at the University of California, Davis. Yorkshire pigs (60–70 kg) were purchased from the UC Davis hog barn facility. After standard anesthesia and under sterile conditions, the carotid artery of the pig was exposed by surgical cutdown with a 5–6 inch incision. Intravenous heparin was administered (150–300 IU/KG IV). Activated clotting times (ACT) was monitored by sampling 0.5 ml of blood from the IV catheter every 30 min. Successive doses of heparin were given if the ACT drops less than twice baseline. At all times, university policy on maximum blood draws was followed. Blood flow to the carotid artery of the pigs was occluded and a segment of the artery was removed and replaced with a 4-cm ePTFE graft with 6 mm inner diameter using standard end-to-end anastomosis techniques with 6-0 prolene. After graft placement, blood flow was restored, and hemostasis at the suture line was achieved by using gauze compression. The muscle and skin around the graft was then closed in a 2-layer fashion with absorbable sutures. No anticoagulants were used after implantation. At week 6 after graft implantation, angiography was performed to evaluate the patency of the grafts by using ISOVUE-370 (Iopamidol), a radiopaque contrast agent which contains iodine, a substance that absorbs x-rays. The pigs were then euthanized by an intravenous injection of pentobarbital (100 mg/kg), and the grafts were explanted, rinsed with PBS for histological analysis.

2.13. Porcine carotid artery-jugular vein arteriovenous graft model

All animal procedures were approved by the Institutional Animal Care and Use Committee at the University of California, Davis. Yorkshire pigs (60–70 kg) were purchased from the UC Davis hog barn facility. After standard anesthesia and under sterile conditions, the carotid artery and jugular vein were exposed by surgical cutdown with a 5–6 inch incision. Intravenous heparin was administered (150–300 IU/KG IV). ACT was monitored as described above. Successive doses of heparin were given if the ACT drops less than twice baseline. Blood flow to both the carotid artery and the internal jugular vein was occluded and a 4-cm ePTFE graft with 6 mm inner diameter was placed between the two vessels using standard end-to-side anastomosis techniques with 6-0 prolene. After graft placement, blood flow was restored, and hemostasis at the suture line was achieved by using of gauze compression. The muscle and skin around the graft was then closed. No anticoagulants were used after implantation. At week 4 after graft implantation, angiography was performed to evaluate the patency of the grafts by using PE. The pigs were then euthanized by an intravenous injection of pentobarbital (100 mg/kg), and the vascular grafts were explanted for histological analysis.

2.14. Histological analysis

The explanted grafts were fixed with 10% formalin (Thermo Fisher Scientific). The luminal surface of the grafts was visualized by using scanning electron microscope. For the preparation of cross-sections, the grafts were dehydrated by 30% sucrose solution, and embedded in

Optimal Cutting Temperature (OCT) compound (Thermo Fisher Scientific). 10 μm sections were prepared. Hematoxylin and eosin (H&E) staining was performed to quantify the thickness of the thrombosis and intimal hyperplasia. Immunofluorescence staining with anti-CD31 antibody (Abcam) and the relevant secondary antibodies (Life Technologies) was performed to evaluate the endothelial coverage on the graft by *en face* staining of the luminal surface of the grafts. Images were captured using the Olympus IX81 microscope. The endothelial coverage rate was defined as the percentage (%) of the $CD31^+$ portion in relation to the total surface area of the graft. Measurement and quantification of endothelial coverage rate on the grafts was performed using ImageJ and Prism.

2.15. Statistical analysis

All quantitative experiments were done in triplicate unless otherwise indicated. Numbers of biological replicates (n) and technical replicates are indicated in figure captions. GraphPad Prism was used for statistical analysis. Student's two-tailed independent *t*-test was used to determine differences between two groups. Comparison of more than two groups were performed using one-way analysis of variance (ANOVA) followed by Tukey's multiple comparisons. Grouped data were analyzed by two-way ANOVA followed by Tukey's multiple comparisons. A p-value less than 0.05 indicates significant difference between samples in comparison.

3. Results

3.1. Construction and characterization of parylene-PEG-LXW7 coated ePTFE grafts

Parylene-PEG-LXW7 (PPL) coating on clinical grade ePTFE grafts was completed in three steps. First, parylene-A, a polymer of p-xylene with primary amine groups (amino- [2,2]paracyclophane), was coated on the ePTFE surface to construct parylene-A coated ePTFE (P-ePTFE) graft using CVD to introduce amino groups onto the inert ePTFE surface (Fig. 1B, C, D). Second, an azide-containing PEG hydrophilic linker (azido-PEG12-NHS ester) was conjugated to the primary amine groups on the P-ePTFE via succinimidyl ester to construct parylene-PEG coated ePTFE (PP-ePTFE) graft (Fig. 1D). Finally, by using a LXW7 derivative, LXW7-DBCO that is LXW7 with a dibenzocyclooctyne group (Fig. S1), LXW7 was covalently ligated to the azide group of the PP-ePTFE surface via Cu-free click chemistry to construct parylene-PEG-LXW7 coated e-PTFE (PPL-ePTFE) graft (Fig. 1D). The parylene-A coated on the ePTFE graft surface was characterized by using the ninhydrin colorimetric assay for amine group detection, and the results showed that the P-ePTFE graft surface was uniformly purple, indicating that parylene-A was uniformly coated on the ePTFE graft surface (Fig. 1C). Coating thicknesses of parylene-A measured using ellipsometry and profilometry on a simultaneously coated Si wafer was about 110 nm (Fig. S2). The PPL coating on the ePTFE graft surface was evaluated step by step using XPS (Fig. 1E). On unmodified ePTFE graft surface, an obvious fluorin (F) peak was present, but no nitrogen peak. On the P-ePTFE graft surface, the fluorin peak disappeared, and the new nitrogen (N) peak was present around 400 eV, which indicating parylene-A was coated successfully onto the ePTFE surface. Subsequently, following PEG linker and LXW7 conjugated to P-ePTFE graft surface, the N peak increased accordingly indicating the PEG linker and LXW7 were successfully conjugated onto the P-ePTFE graft surface. Overall, the XPS results qualitatively confirmed that the PPL coating was successfully conducted on clinical grade ePTFE grafts. Additionally, the AAA was performed to further quantify the LXW7 modified on the ePTFE grafts. The results showed the consistent LXW7 density on the proximal, middle, or distal portion of the LXW7 coated graft, which indicating the LXW7 coating was uniform along the graft lumen (Table 1). According to the AAA results, a very small amount of LXW7 molecules was modified on the graft surface (~40 nmol per cm^2 of the graft surface and total ~180 nmol per graft), which would have minimal impact on other organs. To further confirm the cytotoxicity of the PPL coating, we evaluated the toxicity of the PPL coating on ECFCs. The results showed no significant difference between the ECFCs incubated with or without PPL-ePTFE grafts, which indicated that the PPL coating did not cause any toxicity to the cells (Fig. S3). To evaluate the effect of the PPL coating on the physical properties of the ePTFE graft, tensile strength was measured, and we found no significant difference between the ePTFE grafts, P-ePTFE grafts, PP-ePTFE grafts and PPL-ePTFE grafts (Fig. S4). The contact angle measurement was performed to determine the changes in wettability of the prepared graft surfaces. The results showed the contact angles of PP-ePTFE and PPL-ePTFE grafts was significantly decreased compared to the contact angles of ePTFE and P-ePTFE grafts (Fig. S5). Furthermore, PT, APTT, and hemolysis tests were performed to evaluate the PPL coating. The results showed no significant difference between the different groups (Figs. S6 and S7), which indicating the PPL coating processing designed in this study has no effect on the blood coagulation and destruction of red blood cells.

Table 1
AAA of ePTFE grafts conjugated with LXW7 (cGRGDdvc).

Amino acids	Proximal (nmol/cm^2)		Middle (nmol/cm^2)		Distal (nmol/cm^2)	
	Uncoated	LXW7	Uncoated	LXW7	Uncoated	LXW7
Asp	0.000	83.822	0.000	83.776	0.000	83.961
Gly	0.000	84.893	0.000	84.683	0.000	84.882
Val	0.000	42.241	0.000	42.166	0.000	42.221
Lys	0.000	42.582	0.000	41.883	0.000	42.353
Arg	0.000	42.596	0.000	42.231	0.000	42.673

3.2. PPL coating suppresses adhesion and activation of platelets and improves adhesion and proliferation of EPC on ePTFE grafts

The overall scheme of the function of the PPL-ePTFE grafts on platelet adhesion, EPC adhesion and proliferation was shown in Fig. 2A. The results showed PP-ePTFE and PPL-ePTFE grafts significantly reduced the platelet adhesion compared to the ePTFE and P-ePTFE grafts, and no significant difference was noticed between the PP-ePTFE grafts and PPL-ePTFE grafts (Fig. 2B and C), which demonstrated the PEG modification included in the PPL coating suppressed the platelet adhesion on ePTFE grafts, and the LXW7 modification included in the PPL coating did not increase additional platelet adhesion on the grafts. In addition, the representative SEM images of the platelets adhered on the surfaces, are shown in Fig. S8. On the ePTFE and P-ePTFE graft surfaces, the spread morphology of the activated platelets can be clearly observed. In contrast, on the PP-ePTFE and PPL-ePTFE graft surfaces, and the morphology of the adhered platelets indicated the resting and round shape. Human ECFCs, are also often referred to as outgrowth endothelial cells (OECs) and a subtype of EPCs, were used to evaluate the EPC adhesion and proliferation on different grafts [55]. The results showed that the PPL-ePTFE grafts significantly improved ECFC adhesion (Fig. 2B, D) and proliferation (Fig. 2E and F) compared to the ePTFE, P-ePTFE, PP-ePTFE grafts. To further evaluate whether PPL coating was also applicable to other vascular devices, same PPL coating procedure was applied onto the surfaces of clinical grade bare-metal stents and valves, and the platelet adhesion, ECFC adhesion and proliferation were evaluated on the stents and valves: parylene-A coated stents and valves (P-stent and P-valve), parylene-PEG coated stents and valves (PP-stent and PP-valve) and parylene-PEG-LXW7 coated stents and valves (PPL-stent and PPL-valve). PP-stents and PPL-stents significantly reduced the platelet adhesion compared to the unmodified stents and P-stents, and no significant difference was seen between the PP-stents and PPL-stents. The PPL-stents significantly improved ECFC adhesion and proliferation compared to the unmodified stents, P-stents, PP-stents

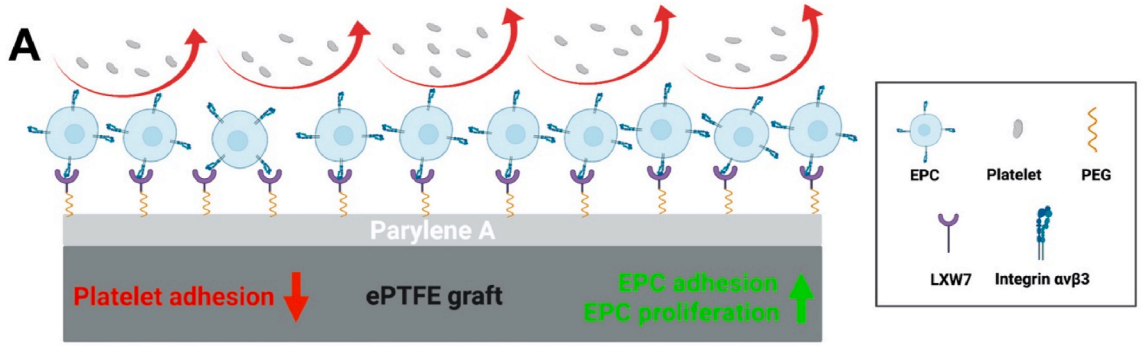

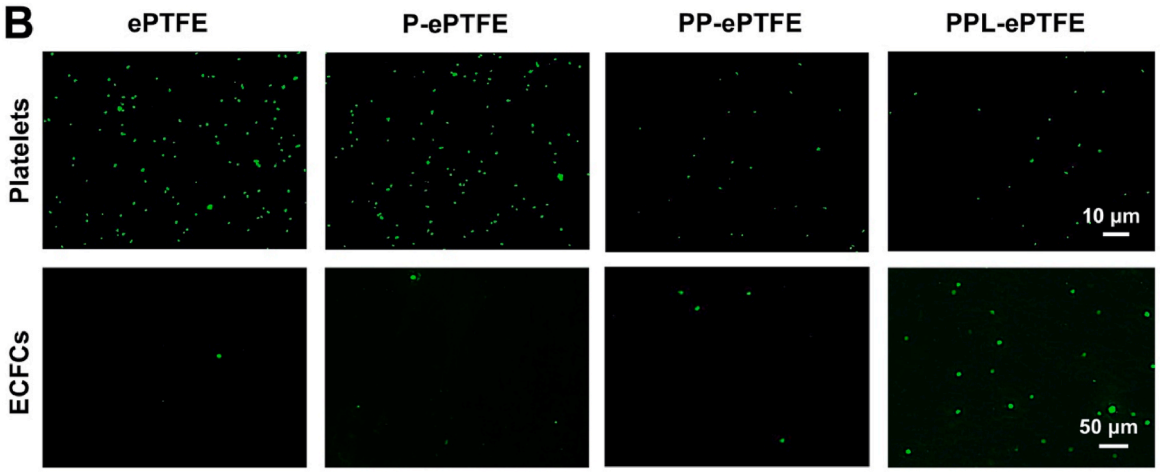

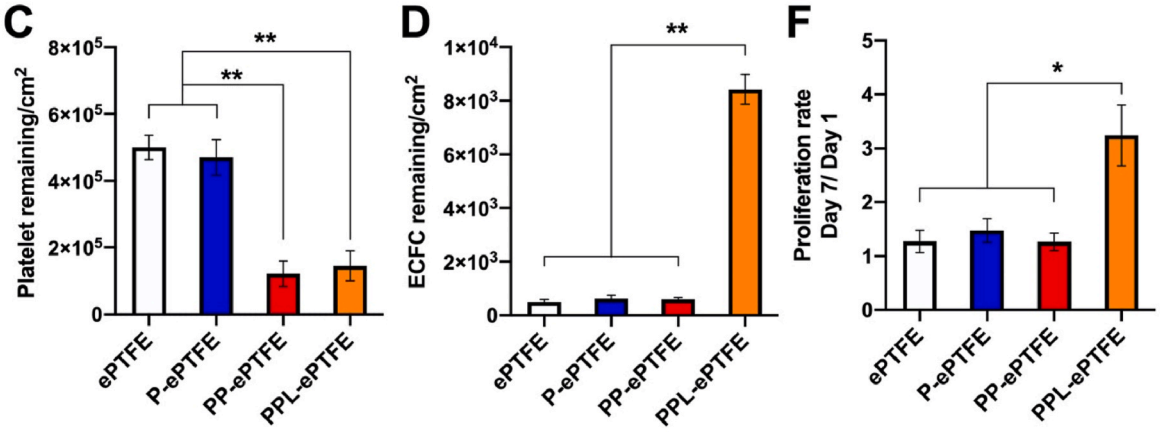

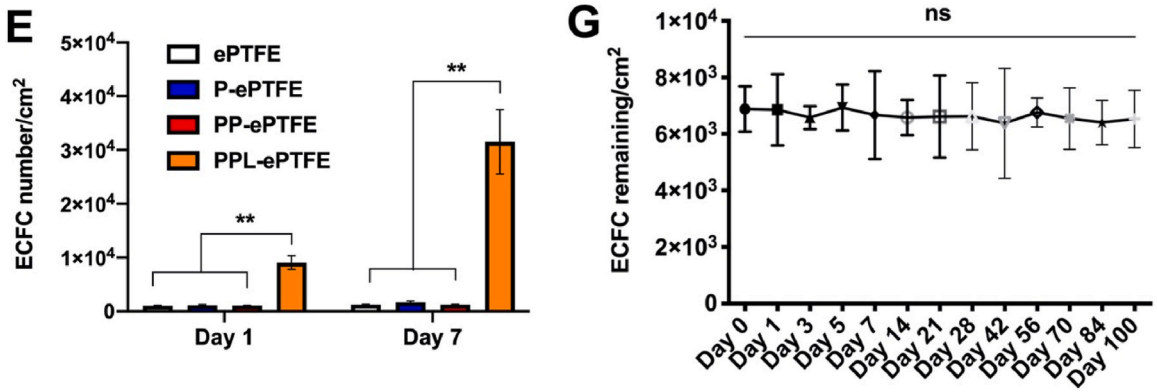

(caption on next page)

Fig. 2. The functionality and long-term serum stability of PPL-ePTFE grafts for platelet adhesion, and EPC adhesion and proliferation. (A) The overall scheme of the functions of PPL-ePTFE grafts on platelet adhesion, EPC adhesion and proliferation. (B) Adhesion of Calcein-AM stained platelets on ePTFE, P-ePTFE, PP-ePTFE and PPL-ePTFE grafts. Scale bar = 10 μm. Adhesion of GFP labelled ECFCs on ePTFE, P-ePTFE, PP-ePTFE and PPL-ePTFE grafts. Scale bar = 50 μm. (C) Quantification of platelet adhesion on the surface of different grafts. (D) Quantification of ECFC adhesion on the surface of different grafts. (E) Quantification of ECFC proliferation on the surface of different grafts on day 1 and day 7 after seeding. (F) Quantification of ECFC proliferation rate from day 1 to day 7 (day 7/day 1) on different grafts. (G) Stability and functionality of PPL coating in human serum for 100 days, characterized by ECFC adhesion on the PPL-ePTFE grafts. Data were expressed as mean ± standard deviation: *$p < 0.05$, **$p < 0.01$ ($n = 6$).

(Fig. S9). PP-valves and PPL-valves significantly reduced the platelet adhesion compared to the unmodified valves and P-valves, and no significant difference was found between the PP-valves and PPL-valves. The PPL-valves significantly improved ECFC adhesion and proliferation compared to the unmodified valves, P-valves, PP-valves (Fig. S10). The results were consistent with the PPL coating on ePTFE grafts. These results indicate that the PPL coating holds the promise for suppressing platelet adhesion and promoting EPC adhesion and proliferation on various prosthetic vascular devices.

3.3. PPL coating maintains long-term functionality in human serum

To evaluate the long-term functionality of PPL coating in serum, the PPL-ePTFE grafts were incubated in the human serum for 100 days, and ECFC adhesion on the grafts was tested at different time points. The results showed that there was no significant decrease of ECFC adhesion for 100 days (Fig. 2G), suggesting that the PPL coating can maintain long-term stability and function in the human serum.

3.4. PPL-ePTFE grafts suppress platelet aggregation, thrombosis and intimal hyperplasia and promote rapid endothelialization and patency in the porcine carotid artery interposition model

The ePTFE grafts (n = 5) and PPL-ePTFE grafts (n = 5) were implanted into 10 pigs right carotid artery as an interposition graft in each pig (Fig. 3A) for 6 weeks. All the surgery was completed in UC Davis large animal facility. After surgery, all the pigs received standard animal care in UC Davis large animal facility and remained survival till 6 weeks. No signs of infection or illness was seen in any of the animals. The grafts were explanted at week 6 after implantation, and the patency of the grafts was determined using angiography. The results showed all the ePTFE grafts and PPL-ePTFE grafts were patent (Fig. 3B and C). The ePTFE grafts and PPL-ePTFE grafts were cut longitudinally open and the macroscopical images of the luminal surface showed that the PPL-ePTFE grafts presented almost no thrombosis, but visible thrombosis occurred on luminal surface of the ePTFE grafts (Fig. 3D). We observed some scar tissue formation surrounding the outside of the implanted grafts, but the scar formation did not seem to have affected the inner surface of the grafts. The explanted grafts were cut into 3 segments: proximal section, middle section, and distal section. Histological analysis of the cross sections of the different sections was performed to further evaluate the explanted grafts. The H&E staining results confirmed the ePTFE grafts with visible thrombosis and intimal hyperplasia (Fig. 3E). Graft patency area, which is defined as percentage (%) the luminal areas of the grafts without thrombosis or neointimal hyperplasia, was measured and quantified on the 3 different segments of all the 5 ePTFE grafts and 5 PPL-ePTFE grafts from the 10 pigs. The results confirmed that the PPL grafts possessed significantly higher patency area compared to the ePTFE grafts (Fig. 3F). The luminal surfaces of the explanted grafts were further analyzed by using SEM at three different positions (Fig. 3G): near anastomosis site (a), the graft midpoint (c), and a site between the anastomosis site and graft midpoint (b). The results showed visible platelet adhesion and aggregation (white arrows) and red cell clumps on the luminal surface of ePTFE grafts, whereas only rare single platelets were observed on the luminal surface of PPL-ePTFE grafts, demonstrating the PPL-ePTFE graft surface possesses the ability to inhibit platelet adhesion and aggregation (Fig. 3G). On the other hand, the luminal surfaces of PPL-ePTFE grafts showed confluent and uniform cellular coverage (red arrows), while almost no cell coverage on the luminal surfaces of ePTFE grafts (Fig. 3G). To further characterize the phenotype of cell coverage on the luminal surfaces of grafts, the luminal surfaces of the explanted grafts was evaluated by immunofluorescence staining with anti-CD31 antibody. The *en face* staining of luminal surface of the grafts confirmed $CD31^+$ EC coverage on a large proportion of the luminal surface of the PPL-ePTFE grafts, whereas only rare $CD31^+$ ECs were observed on the luminal surface of the ePTFE grafts (Fig. 3H). High magnification images of the *en face* staining showed mature confluent endothelial layer on the luminal surface of the PPL-ePTFE grafts, whereas only rare random EC adhesion on the luminal surface of the ePTFE grafts was found (Fig. 3H). Quantification of the endothelial coverage rate of the luminal surface of the grafts showed significant higher endothelial coverage area on the luminal surfaces of the PPL-ePTFE grafts, compared to the ePTFE grafts (Fig. 3I). These results demonstrate the PPL-ePTFE grafts possess remarkable capability in resisting platelet adhesion and aggregation, preventing thrombosis and intimal hyperplasia, and promoting endothelialization in the porcine carotid artery interposition model (Fig. 3J).

3.5. PPL-ePTFE grafts suppress platelet aggregation, thrombosis and intimal hyperplasia and promote rapid endothelialization and patency in the porcine carotid artery-jugular vein arteriovenous graft model

The ePTFE grafts (n = 5) and PPL-ePTFE grafts (n = 5) were implanted between the carotid artery and the internal jugular vein of 10 pigs (Fig. 4A) for 4 weeks. All the surgeries were completed in UC Davis large animal facility. After surgery, all the pigs received standard animal care in UC Davis large animal facility and remained survival till 4 weeks. No signs of infection or illness was seen in any of the animals. The grafts were explanted at week 4 after implantation, and the patency of the grafts was determined using angiography. All the 5 PPL-ePTFE grafts were patent (100%), whereas only 3 of the 5 ePTFE grafts were patent (60%) (Fig. 4B and C). The explanted graft-venous anastomosis was cut along the two dotted lines shown in Fig. 4D to produce cross-sections for histologic analysis. The representative macroscopical images of the patent ePTFE grafts and PPL-ePTFE grafts showed a mass of thrombosis on the luminal surface of the ePTFE grafts, and only a few areas were covered with thrombosis on the luminal surface of the PPL-ePTFE graft (Fig. 4E). We observed some scar tissue formation surrounding the outside of the implanted grafts, but the scar formation did not seem to have affected the inner surface of the grafts. The H&E staining (Fig. 4F) of the cross-sections showed significant lower of thrombosis (Fig. 4G) and intimal hyperplasia (Fig. 4H) at the graft-venous anastomosis of the PPL-ePTFE grafts, compared to the ePTFE grafts. The area of thrombosis and neointimal hyperplasia was measured on the H&E images using ImageJ and quantified on the 3 patent ePTFE grafts and 5 patent PPL-ePTFE grafts. The luminal surfaces of the explanted grafts were analyzed by using SEM to determine the morphology at three different positions of the implanted graft (Fig. 5A). The luminal surface of ePTFE graft showed obvious platelet adhesion and aggregation (white arrows) and red cell clumps, whereas only rare single platelets were observed on the PPL-ePTFE grafts (Fig. 5A). On the other hand, the luminal surfaces of PPL-ePTFE grafts showed confluent and uniform cell coverage (red arrows), while almost no cell coverage was seen on the luminal surfaces of ePTFE grafts (Fig. 5A). To further analyze the cell coverage and phenotype on the luminal surface of grafts, the luminal surface of the explanted grafts was evaluated by immunofluorescence staining with

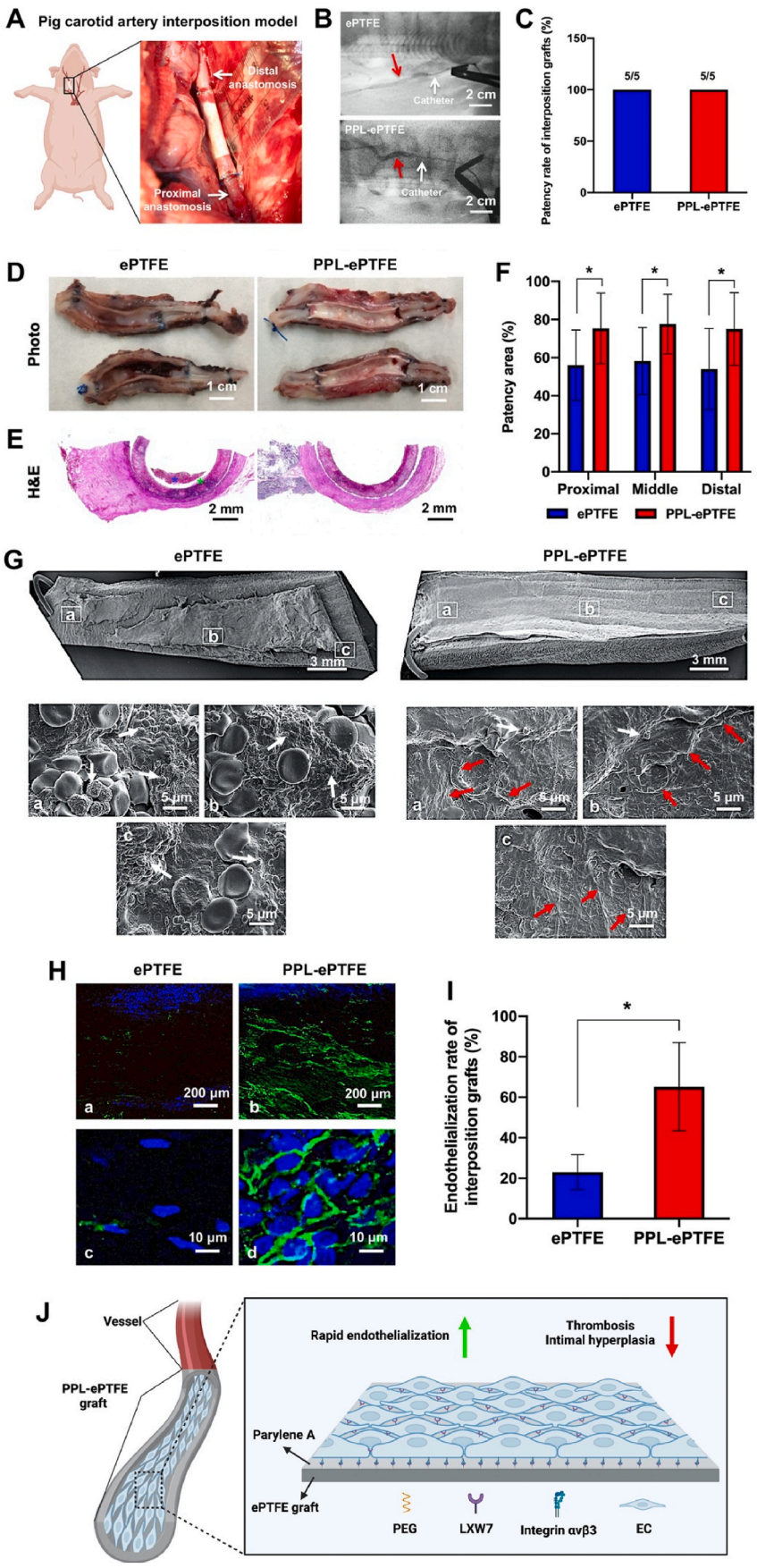

Fig. 3. Evaluation of the functions of PPL-ePTFE grafts in the porcine carotid artery interposition model after 6 weeks of implantation. (A) An representative intraoperative macroscopical image of the implanted graft showed no bleeding and leakage. (B) Angiography images of the ePTFE graft and patent PPL-ePTFE graft at week 6 after implantation. The red arrows indicate the positions of the implanted grafts. The white arrows indicate the catheter used for the contrast agent injection. Scale bar = 2 cm. (C) The patency rates of the ePTFE grafts and PPL-ePTFE grafts. (D) Representative macroscopical images of the luminal surface of the explanted ePTFE grafts and PPL-ePTFE grafts. Scale bar = 1 cm. (E) H&E staining of the cross-section at the middle portion of the explanted ePTFE grafts and PPL-ePTFE grafts. Blue star indicates the thrombosis, and the green star indicates the neointimal hyperplasia. Scale bar = 2 mm. (F) Quantification of the patency area of the explanted ePTFE grafts and PPL-ePTFE grafts. Data were expressed as mean ± standard deviation: *$p < 0.05$ (n = 5). (G) SEM images of the luminal surfaces of the explanted grafts after 6 weeks of implantation. Images at low magnification showed the general appearance of the luminal surfaces of the grafts. Scale bar = 3 mm. Images of a, b, and c with high magnification correspond to the three white boxed areas from the low magnification images. White arrows indicate the platelet adhesion and aggregation, and the red arrows indicate the cell coverage. Scale bar = 5 μm. (H) *En face* immunofluorescence staining of luminal surface of the explanted ePTFE grafts and PPL-ePTFE grafts. Green for CD31 immunostaining, and the blue for the nuclear staining (DAPI). Scale bar = 200 μm. Representative images at low magnification (a, b) showed EC coverage of the luminal surface of the grafts, and images at high magnification (c, d) showed the morphology of the cells on the luminal surface. Scale bar = 10 μm. (I) Quantification of endothelial coverage area of the ePTFE grafts and PPL-ePTFE grafts. Data were expressed as mean ± standard deviation: *$p < 0.05$ (n = 5). (J) The mechanism of action of the PPL conformal coating to promote endothelization and suppress platelet aggregation, thrombosis, and intimal hyperplasia.

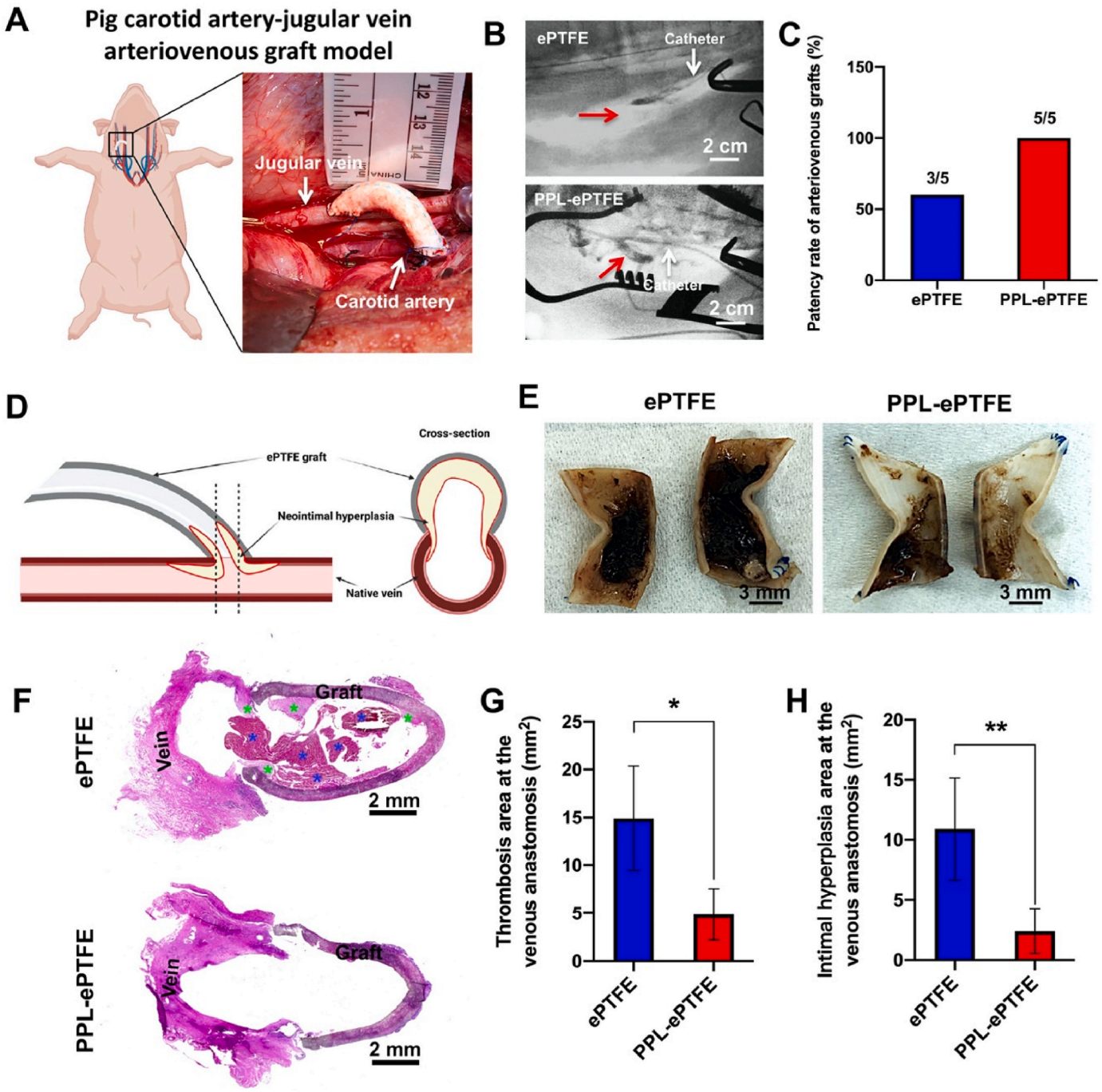

Fig. 4. The PPL-ePTFE grafts improve patency, suppress thrombosis and neointimal hyperplasia in the porcine carotid artery-jugular vein arteriovenous graft model after 4 weeks of implantation. (A) A representative macroscopical image showed that implanted grafts had no bleeding and leakage. (B) Angiography images of the occluded ePTFE graft and patent PPL-ePTFE graft. The red arrows indicate the positions of the implanted grafts. The white arrows indicate the catheter used for the contrast agent injection. Scale bar = 2 cm. (C) The patency rates of the ePTFE grafts and the PPL-ePTFE grafts. (D) Schematic diagram of the graft-vein anastomosis. The graft-venous anastomosis was cut along the two dotted lines to produce cross-sections for histologic analysis. (E) Representative macroscopical images of the explanted patent ePTFE graft and PPL-ePTFE graft. Scale bar = 3 mm. (F) H&E staining of cross-section of the explanted patent ePTFE graft and PPL-ePTFE graft. Blue stars indicate the thrombosis, and the green stars indicate the neointimal hyperplasia. Scale bar = 2 mm. (G) Quantitation of the thrombosis area of the patent ePTFE grafts and PPL-ePTFE grafts. (H) Quantitation of the neointimal hyperplasia area of the patent ePTFE grafts and PPL-ePTFE grafts. Data were expressed as mean ± standard deviation: *$p < 0.05$, **$p < 0.01$ ($n = 3$ for patent ePTFE grafts, and $n = 5$ for patent PPL-ePTFE grafts).

CD31 antibody. The *en face* staining of the luminal surface of the grafts showed $CD31^+$ EC coverage on a large proportion of the PPL-ePTFE graft, whereas only minimal endothelial coverage was observed on the luminal surface of the ePTFE graft (Fig. 5B). The high magnification images showed the mature endothelial cell morphology with typical endothelial tight junctions, whereas only rare random EC adhesion was seen on the luminal surface of the ePTFE graft (Fig. 5B). The quantification results showed significant higher of endothelial coverage on the luminal surfaces of the PPL-ePTFE grafts compared to the ePTFE grafts (Fig. 5C). These results obtained from the porcine carotid artery-jugular vein arteriovenous graft model were consistent with that from the porcine carotid artery interposition model, further demonstrating the

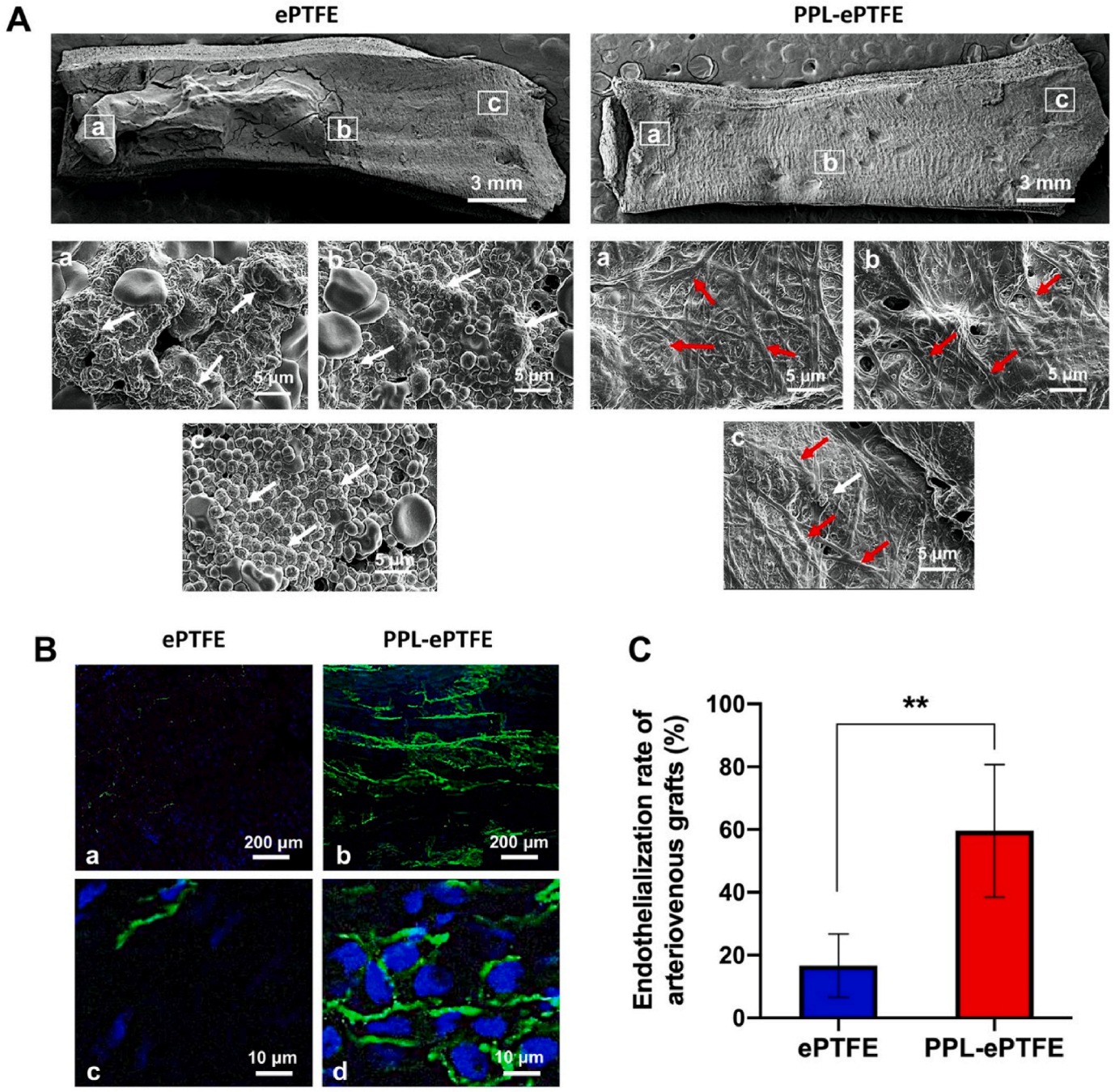

Fig. 5. The PPL-ePTFE grafts promote rapid endothelialization and suppress platelet aggregation in the porcine carotid artery-jugular vein arteriovenous graft model after 4 weeks of implantation. (A) SEM images for the luminal surfaces of the explanted grafts after 4 weeks of implantation. Images at low magnification showed the general appearance of the luminal surfaces of grafts. Scale bar = 3 mm. Images of (a), (b), and (c) with high magnification correspond to the three boxed areas from the low magnification image. White arrows indicate the platelet adhesion and aggregation, and the red arrows indicate the cell coverage. Scale bar = 5 μm. (B) *En face* immunofluorescence staining of longitudinal sections of ePTFE grafts and PPL-ePTFE grafts. Green for CD31 immunostaining, and the blue for the nuclear staining (DAPI). Scar bar = 200 μm. Images at low magnification (a, b) showed the EC coverage. Images at high magnification (c, d) showed the mature confluent endothelial layer. Scale bar = 10 μm. (C) Quantification of endothelial coverage area of the ePTFE grafts and PPL-ePTFE grafts. Data were expressed as mean ± standard deviation: $^{**}p < 0.01$ (n = 3 for patent ePTFE grafts, and n = 5 for patent PPL-ePTFE grafts).

prominent regenerative capacity of the PPL-ePTFE grafts in platelet resistance, rapid endothelialization and prevention of thrombosis and intimal hyperplasia.

4. Discussion

The bioactive parylene-based conformal coating (PPL coating) developed in this study covalently presenting an antifouling PEG linker [56] and an integrin-based ligand LXW7 with high binding affinity and specificity to EPCs [32,33] shed a light to conquer the current challenges of prosthetic vascular devices in clinical applications. Specifically, because of the antifouling PEG linker, the coating suppressed platelet adhesion on the surface of the vascular devices for preventing the early-stage thrombosis before the endothelialization. The PEG linker

also could provide better malleability and more space for LXW7 to efficiently capture circulating EPCs to achieve rapid endothelialization. Because of the integrin-based ligand LXW7, the coating possessed biological resemblance to native ECM and promoted EPC adhesion and proliferation on the prosthetic vascular devices. Overall, at the early stage, we expected that the LXW7 preferentially and specifically recruit EPCs compared to platelets and other types of cells for rapids endothelization. Additionally, the PEG-based molecule, an agent for the inhibition of surface interactions of blood mononuclear cells and platelets [57], was included in the surface modification of the ePTFE graft, which also contributed to reduce the adhesion of platelet and other types of cells at the early stage. At the late stage, the newly formed endothelium will further suppress the adhesion and aggregation of platelets and other types of cells. LXW7 has several advantages over other functional molecules previously investigated to modify the prosthetic vascular devices.

Compared to biomacromolecules, such as CD34 antibodies, that have been used to modify prosthetic vascular devices and tested in clinical trials [58–60], LXW7 is a small integrin-based peptide ligand, which possesses better stability and EPC/EC binding specificity *in vivo*. In Fig. 2G, we revealed LXW7 maintained its function for EPC adhesion for at least 100 days in human serum. Compared to the similar integrin-based ligand RGD peptide [28,61], LXW7 showed higher binding specificity and stronger binding affinity to human primary EPCs and different types of ECs and weaker binding to platelets [32]. Moreover, compared to other approaches for presenting functional molecules onto the surface of prosthetic vascular devices [62,63], parylene-based coating is a FDA-approved, stable and conformal coating approach. In Fig. 1C, we demonstrated this parylene-based coating could form a uniformly distributed foundational layer on the surface of the ePTFE grafts, which will ensure the LXW7 ligand will be evenly distributed on the surface of the prosthetic vascular devices for consistently capturing EPCs/ECs to achieve confluent endothelial coverage on the prosthetic vascular devices. In Fig. 2G, we revealed that this parylene-based coating could be stable in the human serum for at least 100 days. Furthermore, in Fig. 2 and Fig. S9 and Fig. S10, this PPL coating has been demonstrated to be successfully applied to various clinical vascular devices, such as ePTFE grafts, bare-metal stents, and valves, and showed their function in suppressing platelet adhesion and promoting EPC adhesion and proliferation.

Porcine models have been used as representative models for preclinical studies of vascular diseases because of their analogous vascular anatomy, physiology and size with human [64–67]. Based on the current clinical needs for the vascular diseases, we established two clinical disease-related models in pigs to evaluate the function of this coating. One is the carotid artery interposition model, a model for blood vessel bypass and replacement, which is the common treatment approach for a large population of patients with various vascular diseases, such as atherosclerosis, restenosis, and aneurysms. The other model is the carotid artery-jugular vein arteriovenous graft model, which is related to the essential treatment approach for patients with end-stage renal disease who are on chronic hemodialysis. In these two porcine models, the PPL-ePTFE grafts designed in this study significantly suppressed platelet aggregation, thrombosis and neointimal hyperplasia and improved rapid endothelialization and patency, compared to the unmodified conventional ePTFE grafts. Remarkably, at week 4 after implantation in the carotid artery-internal jugular vein arteriovenous graft model, the PPL-ePTFEs grafts achieved 100% patency rate, compared to the literature reported 73% patency rate of the CD34 antibody coated ePTFE grafts [60]. Furthermore, in Figs. 3G and 5A, the SEM results showed the cells adhered and spread on the luminal surface of the PPL-ePTFE grafts confluently and uniformly, which is crucial for tissue remodeling and development, including vascular development [68]. In Figs. 3H and 5B, the *en face* immunofluorescence staining results showed mature confluent endothelial cells on the luminal surface of the PPL-ePTFE graft, which is the symbol of mature endothelium and essential to maintain long-term vascular homeostasis [69]. In this study, we did not include other irrelevant peptides or LXW7 antagonists as controls. Since large animal studies are technically challenging and financially inhibitive, in this first large animal study, we focused on evaluating the function of LXW7 in two clinically relevant disease conditions in the translational porcine models. Also, in our previous study, we have compared the functions of LXW7 to the conventional integrin ligand GRGD peptide and confirmed that LXW7 has stronger binding affinity to primary EPCs/ECs but weaker binding to platelets. In our future studies, we are planning to include the GRGD peptide and a scrambled peptide as controls.

5. Conclusion

This bioactive parylene-based conformal coating will prove to be a major advancement in a variety of areas. It will provide an easy-to-use solution to the issue of lack of functional "living" endothelium on the prosthetic vascular device surface. This coating can be applied to existing medical vascular devices and does not change current clinical practice regarding surgical implantation. This coating would not only benefit patients and hospitals from a healthcare perspective, but also a financial one. Development of a surface conformal coating that increases the long-term performance of vascular devices will in turn lower healthcare costs associated with the vascular device failure or malfunction. Furthermore, the device developed from this project will have significant impact on the methods and technologies for the treatment of vascular diseases. Providing a durable vascular graft with long-term patency and endothelium self-regeneration will allow reliable access to life-saving hemodialysis for patients with renal failure and a durable solution to revascularization for patients with numerous vascular diseases. Our work could also lead to improved treatments for chronic vascular diseases such as coronary artery disease and peripheral artery disease, which may otherwise result in death from ischemic cardiomyopathy, the need for heart transplantation, and limb loss. Although the focus of the current study is on vascular grafts, the same surface coating can be easily applied to a wide range of vascular and endovascular devices, including stents, cardiac valves, ports, and catheters. This bioactive parylene-based conformal coating could also provide a platform for loading various biologics, such as drugs, extracellular vesicles, and biological molecules, onto the surface of the medical devices to improve their regenerative potentials.

Ethics approval and consent to participate

All animal procedures are approved by the Institutional Animal Care and Use Committee at the University of California, Davis.

CRediT authorship contribution statement

Dake Hao: Conceptualization, Data curation, Formal analysis, Investigation, Methodology, Project administration, Resources, Software, Supervision, Writing – original draft. **Jonathan Lin:** Methodology. **Ruiwu Liu:** Data curation, Software. **Christopher Pivetti:** Methodology. **Kaeli Yamashiro:** Methodology. **Linda M. Schutzman:** Methodology. **Junichiro Sageshima:** Writing – review & editing. **Mimmie Kwong:** Writing – review & editing. **Nataliya Bahatyrevich:** Writing – review & editing. **Diana L. Farmer:** Writing – review & editing. **Misty D. Humphries:** Methodology, Writing – review & editing. **Kit S. Lam:** Methodology, Writing – review & editing. **Alyssa Panitch:** Writing – review & editing. **Aijun Wang:** Conceptualization, Supervision, Writing – review & editing.

Declaration of competing interest

AP, KL, and AW are founders in VasoBio Inc, which has a license to the LXW7 technology. Other authors declare no potential conflicts of interest with respect to the authorship and/or publication of this article.

Acknowledgements

This work was in part supported by the UC Davis School of Medicine Dean's Fellowship award, the Science Translation and Innovative Research (STAIR) grant offered by UC Davis Venture Catalyst, the National Heart, Lung, And Blood Institute under Award Number T32 HL086350 and U54HL 119893 through UC BRAID Center for Accelerated Innovation Technology Grant, and California Institute for Regenerative Medicine (CIRM) grant (TRAN3-13332). The authors would also like to thank the Combinatorial Chemistry Shared Resource at University of California Davis for assistance with design and synthesis of peptides and their derivatives. Utilization of this Shared Resource was supported by the UC Davis Comprehensive Cancer Center Support Grant awarded by the National Cancer Institute (P30CA093373).

Appendix A. Supplementary data

Supplementary data to this article can be found online at https://doi.org/10.1016/j.bioactmat.2023.06.014.

References

[1] M. Writing Group, D. Mozaffarian, E.J. Benjamin, A.S. Go, D.K. Arnett, M.J. Blaha, M. Cushman, S.R. Das, S. de Ferranti, J.P. Despres, H.J. Fullerton, V.J. Howard, M. D. Huffman, C.R. Isasi, M.C. Jimenez, S.E. Judd, B.M. Kissela, J.H. Lichtman, L. D. Lisabeth, S. Liu, R.H. Mackey, D.J. Magid, D.K. McGuire, E.R. Mohler 3rd, C. S. Moy, P. Muntner, M.E. Mussolino, K. Nasir, R.W. Neumar, G. Nichol, L. Palaniappan, D.K. Pandey, M.J. Reeves, C.J. Rodriguez, W. Rosamond, P. D. Sorlie, J. Stein, A. Towfighi, T.N. Turan, S.S. Virani, D. Woo, R.W. Yeh, M. B. Turner, C. American Heart Association Statistics, S. Stroke Statistics, Heart disease and stroke statistics-2016 update: a report from the American heart association, Circulation 133 (4) (2016) e38–e360.

[2] P. Roy-Chaudhury, V.P. Sukhatme, A.K. Cheung, Hemodialysis vascular access dysfunction: a cellular and molecular viewpoint, J. Am. Soc. Nephrol. 17 (4) (2006) 1112–1127.

[3] D.H. Lee, J.M. de la Torre Hernandez, The newest generation of drug-eluting stents and beyond, Eur. Cardiol. 13 (1) (2018) 54–59.

[4] D. Zhi, Q. Cheng, A.C. Midgley, Q. Zhang, T. Wei, Y. Li, T. Wang, T. Ma, M. Rafique, S. Xia, Y. Cao, Y. Li, J. Li, Y. Che, M. Zhu, K. Wang, D. Kong, Mechanically reinforced biotubes for arterial replacement and arteriovenous grafting inspired by architectural engineering, Sci. Adv. 8 (11) (2022), eabl3888.

[5] Z. Huang, Y. Zhang, R. Liu, Y. Li, M. Rafique, A.C. Midgley, Y. Wan, H. Yan, J. Si, T. Wang, C. Chen, P. Wang, M. Shafiq, J. Li, L. Zhao, D. Kong, K. Wang, Cobalt loaded electrospun poly(epsilon-caprolactone) grafts promote antibacterial activity and vascular regeneration in a diabetic rat model, Biomaterials 291 (2022), 121901.

[6] H. Miyachi, J.W. Reinhardt, S. Otsuru, S. Tara, H. Nakayama, T. Yi, Y.U. Lee, S. Miyamoto, T. Shoji, T. Sugiura, C.K. Breuer, T. Shinoka, Bone marrow-derived mononuclear cell seeded bioresorbable vascular graft improves acute graft patency by inhibiting thrombus formation via platelet adhesion, Int. J. Cardiol. 266 (2018) 61–66.

[7] Z.M. Ruggeri, G.L. Mendolicchio, Adhesion mechanisms in platelet function, Circ. Res. 100 (12) (2007) 1673–1685.

[8] E.I. Lev, D. Leshem-Lev, A. Mager, H. Vaknin-Assa, N. Harel, Y. Zimra, T. Bental, G. Greenberg, D. Dvir, A. Solodky, A. Assali, A. Battler, R. Kornowski, Circulating endothelial progenitor cell levels and function in patients who experienced late coronary stent thrombosis, Eur. Heart J. 31 (21) (2010) 2625–2632.

[9] J.D. Pearson, Endothelial cell function and thrombosis, Baillieres Best Pract. Res. Clin. Haematol. 12 (3) (1999) 329–341.

[10] V.W. van Hinsbergh, The endothelium: vascular control of haemostasis, Eur. J. Obstet. Gynecol. Reprod. Biol. 95 (2) (2001) 198–201.

[11] G.M. Rubanyi, The role of endothelium in cardiovascular homeostasis and diseases, J. Cardiovasc. Pharmacol. 22 (Suppl 4) (1993) S1–S14.

[12] A. Harding, E. Cortez-Toledo, N.L. Magner, J.R. Beegle, D.P. Coleal-Bergum, D. Hao, A. Wang, J.A. Nolta, P. Zhou, Highly efficient differentiation of endothelial cells from pluripotent stem cells requires the MAPK and the PI3K pathways, Stem Cell. 35 (4) (2017) 909–919.

[13] W. Zeng, C. Wen, Y. Wu, L. Li, Z. Zhou, J. Mi, W. Chen, M. Yang, C. Hou, J. Sun, C. Zhu, The use of BDNF to enhance the patency rate of small-diameter tissue-engineered blood vessels through stem cell homing mechanisms, Biomaterials 33 (2) (2012) 473–484.

[14] Y.B. Lee, Y.M. Shin, J.H. Lee, I. Jun, J.K. Kang, J.C. Park, H. Shin, Polydopamine-mediated immobilization of multiple bioactive molecules for the development of functional vascular graft materials, Biomaterials 33 (33) (2012) 8343–8352.

[15] W. Zeng, W. Yuan, L. Li, J. Mi, S. Xu, C. Wen, Z. Zhou, J. Xiong, J. Sun, D. Ying, M. Yang, X. Li, C. Zhu, The promotion of endothelial progenitor cells recruitment by nerve growth factors in tissue-engineered blood vessels, Biomaterials 31 (7) (2010) 1636–1645.

[16] K. Gao, P. Kumar, E. Cortez-Toledo, D. Hao, L. Reynaga, M. Rose, C. Wang, D. Farmer, J. Nolta, J. Zhou, P. Zhou, A. Wang, Potential long-term treatment of hemophilia A by neonatal co-transplantation of cord blood-derived endothelial colony-forming cells and placental mesenchymal stromal cells, Stem Cell Res. Ther. 10 (1) (2019) 34.

[17] D. Hao, C. He, B. Ma, L. Lankford, L. Reynaga, D.L. Farmer, F. Guo, A. Wang, Hypoxic preconditioning enhances survival and proangiogenic capacity of human first trimester chorionic villus-derived mesenchymal stem cells for fetal tissue engineering, Stem Cell. Int. 2019 (2019), 9695239.

[18] L. Lu, H. Chen, D. Hao, X. Zhang, F. Wang, The functions and applications of A7R in anti-angiogenic therapy, imaging and drug delivery systems, Asian J. Pharm. Sci. 14 (6) (2019) 595–608.

[19] L. Ramasubramanian, S. Du, S. Gidda, N. Bahatyrevich, D. Hao, P. Kumar, A. Wang, Bioengineering extracellular vesicles for the treatment of cardiovascular diseases, Adv Biol (Weinh) 6 (10) (2022), e2200087.

[20] A. Stahl, D. Hao, J. Barrera, D. Henn, S. Lin, S. Moeinzadeh, S. Kim, W. Maloney, G. Gurtner, A. Wang, Y.P. Yang, A bioactive compliant vascular graft modulates macrophage polarization and maintains patency with robust vascular remodeling, Bioact. Mater. 19 (2023) 167–178.

[21] H. Yan, Q. Cheng, J. Si, S. Wang, Y. Wan, X. Kong, T. Wang, W. Zheng, M. Rafique, X. Li, J. He, A.C. Midgley, Y. Zhu, K. Wang, D. Kong, Functionalization of in vivo tissue-engineered living biotubes enhance patency and endothelization without the requirement of systemic anticoagulant administration, Bioact. Mater. 26 (2023) 292–305.

[22] L. Goldbloom-Helzner, D. Hao, A. Wang, Developing regenerative treatments for developmental defects, injuries, and diseases using extracellular matrix collagen-targeting peptides, Int. J. Mol. Sci. 20 (17) (2019) 4072.

[23] D. Hao, R. Liu, T.G. Fernandez, C. Pivetti, J.E. Jackson, E.S. Kulubya, H.J. Jiang, H. Y. Ju, W.L. Liu, A. Panitch, K.S. Lam, J.K. Leach, D.L. Farmer, A. Wang, A bioactive material with dual integrin-targeting ligands regulates specific endogenous cell adhesion and promotes vascularized bone regeneration in adult and fetal bone defects, Bioact. Mater. 20 (2023) 179–193.

[24] D. Hao, J.M. Lopez, J. Chen, A.M. Iavorovschi, N.M. Lelivelt, A. Wang, Engineering extracellular microenvironment for tissue regeneration, Bioengineering (Basel) 9 (5) (2022) 202.

[25] D. Hao, L. Lu, H. Song, Y. Duan, J. Chen, R. Carney, J.J. Li, P. Zhou, J. Nolta, K. S. Lam, J.K. Leach, D.L. Farmer, A. Panitch, A. Wang, Engineered extracellular vesicles with high collagen-binding affinity present superior in situ retention and therapeutic efficacy in tissue repair, Theranostics 12 (13) (2022) 6021–6037.

[26] D. Hao, B. Ma, C. He, R. Liu, D.L. Farmer, K.S. Lam, A. Wang, Surface modification of polymeric electrospun scaffolds via a potent and high-affinity integrin alpha4beta1 ligand improved the adhesion, spreading and survival of human chorionic villus-derived mesenchymal stem cells: a new insight for fetal tissue engineering, J. Mater. Chem. B 8 (8) (2020) 1649–1659.

[27] S. Lazar, S. Mor, J. Chen, D. Hao, A. Wang, Bioengineered extracellular vesicle-loaded bioscaffolds for therapeutic applications in regenerative medicine, Extracell Vesicles. Circ. Nucl. Acids 2 (2021) 175–178.

[28] R. Blindt, F. Vogt, I. Astafieva, C. Fach, M. Hristov, N. Krott, B. Seitz, A. Kapurniotu, C. Kwok, M. Dewor, A.K. Bosserhoff, J. Bernhagen, P. Hanrath, R. Hoffmann, C. Weber, A novel drug-eluting stent coated with an integrin-binding cyclic Arg-Gly-Asp peptide inhibits neointimal hyperplasia by recruiting endothelial progenitor cells, J. Am. Coll. Cardiol. 47 (9) (2006) 1786–1795.

[29] W. Zheng, Z. Wang, L. Song, Q. Zhao, J. Zhang, D. Li, S. Wang, J. Han, X.L. Zheng, Z. Yang, D. Kong, Endothelialization and patency of RGD-functionalized vascular grafts in a rabbit carotid artery model, Biomaterials 33 (10) (2012) 2880–2891.

[30] S.P. Jackson, The growing complexity of platelet aggregation, Blood 109 (12) (2007) 5087–5095.

[31] J. Sanchez-Cortes, M. Mrksich, The platelet integrin alphaIIbbeta3 binds to the RGD and AGD motifs in fibrinogen, Chem. Biol. 16 (9) (2009) 990–1000.

[32] D. Hao, W. Xiao, R. Liu, P. Kumar, Y. Li, P. Zhou, F. Guo, D.L. Farmer, K.S. Lam, F. Wang, A. Wang, Discovery and characterization of a potent and specific peptide ligand targeting endothelial progenitor cells and endothelial cells for tissue regeneration, ACS Chem. Biol. 12 (4) (2017) 1075–1086.

[33] D. Hao, Y. Fan, W. Xiao, R. Liu, C. Pivetti, T. Walimbe, F. Guo, X. Zhang, D. L. Farmer, F. Wang, A. Panitch, K.S. Lam, A. Wang, Rapid endothelialization of small diameter vascular grafts by a bioactive integrin-binding ligand specifically targeting endothelial progenitor cells and endothelial cells, Acta Biomater. 108 (2020) 178–193.

[34] D. Hao, R. Liu, K. Gao, C. He, S. He, C. Zhao, G. Sun, D.L. Farmer, A. Panitch, K. S. Lam, A. Wang, Developing an injectable nanofibrous extracellular matrix hydrogel with an integrin alphavbeta3 ligand to improve endothelial cell survival, engraftment and vascularization, Front. Bioeng. Biotechnol. 8 (2020) 890.

[35] D. Hao, H.S. Swindell, L. Ramasubramanian, R. Liu, K.S. Lam, D.L. Farmer, A. Wang, Extracellular matrix mimicking nanofibrous scaffolds modified with mesenchymal stem cell-derived extracellular vesicles for improved vascularization, Front. Bioeng. Biotechnol. 8 (2020) 633.

[36] S. He, T. Walimbe, H. Chen, K. Gao, P. Kumar, Y. Wei, D. Hao, R. Liu, D.L. Farmer, K.S. Lam, J. Zhou, A. Panitch, A. Wang, Bioactive extracellular matrix scaffolds engineered with proangiogenic proteoglycan mimetics and loaded with endothelial progenitor cells promote neovascularization and diabetic wound healing, Bioact. Mater. 10 (2022) 460–473.

[37] H. Song, K. Gao, D. Hao, A. Li, R. Liu, B. Anggito, B. Yin, Q. Jin, V. Dartora, K. S. Lam, L.R. Smith, A. Panitch, J. Zhou, D.L. Farmer, A. Wang, Engineered multi-functional, pro-angiogenic collagen-based scaffolds loaded with endothelial cells promote large deep burn wound healing, Front. Pharmacol. 14 (2023), 1125209.

[38] F.M. Veronese, G. Pasut, PEGylation, successful approach to drug delivery, Drug Discov. Today 10 (21) (2005) 1451–1458.
[39] S.F. Chou, B.A. Caltrider, A. Azghani, P.F. Neuenschwander, Inhibition of platelet adhesion from surface modified polyurethane membranes, Biomed. J. Sci. Tech. Res. 32 (3) (2020) 24988–24993.
[40] K.D. Park, K. Suzuki, W.K. Lee, J.E. Lee, Y.H. Kim, Y. Sakurai, T. Okano, Platelet adhesion and activation on polyethylene glycol modified polyurethane surfaces. Measurement of cytoplasmic calcium, Am. Soc. Artif. Intern. Organs J. 42 (5) (1996) M876–M881.
[41] S.S. Banerjee, N. Aher, R. Patil, J. Khandare, Poly(ethylene glycol)-prodrug conjugates: concept, design, and applications, J. Drug Deliv. 2012 (2012), 103973.
[42] J.K. Dozier, M.D. Distefano, Site-specific PEGylation of therapeutic proteins, Int. J. Mol. Sci. 16 (10) (2015) 25831–25864.
[43] D.J. Kereiakes, The myths of the bare-metal stent, JAMA Cardiol. 3 (11) (2018) 1039–1040.
[44] R.D. Kirkton, H.L. Prichard, M. Santiago-Maysonet, L.E. Niklason, J.H. Lawson, S.L. M. Dahl, Susceptibility of ePTFE vascular grafts and bioengineered human acellular vessels to infection, J. Surg. Res. 221 (2018) 143–151.
[45] M.T. Lam, J.C. Wu, Biomaterial applications in cardiovascular tissue repair and regeneration, Expert Rev. Cardiovasc Ther. 10 (8) (2012) 1039–1049.
[46] L. Brancato, D. Decrop, J. Lammertyn, R. Puers, Surface nanostructuring of parylene-C coatings for blood contacting implants, Materials 11 (7) (2018) 1109.
[47] I. Marei, A. Chester, I. Carubelli, T. Prodromakis, T. Trantidou, M.H. Yacoub, Assessment of parylene C thin films for heart valve tissue engineering, Tissue Eng. Part A 21 (19–20) (2015) 2504–2514.
[48] P.N. Wahjudi, J.H. Oh, S.O. Salman, J.A. Seabold, D.C. Rodger, Y.C. Tai, M. E. Thompson, Improvement of metal and tissue adhesion on surface-modified parylene C, J. Biomed. Mater. Res. 89 (1) (2009) 206–214.
[49] J. Bienkiewicz, Plasma-enhanced parylene coating for medical device applications, Med. Device Technol. 17 (1) (2006) 10–11.
[50] O. Grinberg, M. Natan, A. Lipovsky, A. Varvak, H. Keppner, A. Gedanken, E. Banin, Antibiotic nanoparticles embedded into the Parylene C layer as a new method to prevent medical device-associated infections, J. Mater. Chem. B 3 (1) (2015) 59–64.
[51] L.L.C. Medtech Insight, European Markets for Prosthetic Vascular Grafts, Medtech Insight, Newport Beach, CA, 2006.
[52] A.D. Mason, C.C. Huang, S. Kondo, M.T. Koesdjojo, Y.H. Tennico, V.T. Remcho, J. F. Conley, Synthesis, functionalization, and environmental stabilization of ZnO nanobridge transducers for gas and liquid-phase sensing, Sensor Actuat. B-Chem. 155 (1) (2011) 245–252.
[53] B.J. Jeon, M.H. Kim, J.C. Pyun, Parylene-A coated microplate for covalent immobilization of proteins and peptides, J. Immunol. Methods 353 (1–2) (2010) 44–48.
[54] C.M. Theodorou, A. Taylor, S.Y. Lee, L.M. Cortez, H. Fu, C.D. Pivetti, C. Zhang, A. Stasyuk, D. Hao, P. Kumar, D.L. Farmer, J. Liao, E.G. Brown, Y. Hong, A. Wang, Evaluation of a biodegradable polyurethane patch for repair of diaphragmatic hernia in a rat model: a pilot study, J. Pediatr. Surg. 58 (5) (2023) 964–970.
[55] D.A. Ingram, L.E. Mead, H. Tanaka, V. Meade, A. Fenoglio, K. Mortell, K. Pollok, M. J. Ferkowicz, D. Gilley, M.C. Yoder, Identification of a novel hierarchy of endothelial progenitor cells using human peripheral and umbilical cord blood, Blood 104 (9) (2004) 2752–2760.
[56] Q. Chen, S. Yu, D. Zhang, W. Zhang, H. Zhang, J. Zou, Z. Mao, Y. Yuan, C. Gao, R. Liu, Impact of antifouling PEG layer on the performance of functional peptides in regulating cell behaviors, J. Am. Chem. Soc. 141 (42) (2019) 16772–16780.
[57] A. Sauter, G. Richter, A. Micoulet, A. Martinez, J.P. Spatz, S. Appel, Effective polyethylene glycol passivation for the inhibition of surface interactions of peripheral blood mononuclear cells and platelets, Biointerphases 8 (1) (2013) 14.
[58] G. Nakazawa, J.F. Granada, C.L. Alviar, A. Tellez, G.L. Kaluza, M.Y. Guilhermier, S. Parker, S.M. Rowland, F.D. Kolodgie, M.B. Leon, R. Virmani, Anti-CD34 antibodies immobilized on the surface of sirolimus-eluting stents enhance stent endothelialization, JACC Cardiovasc. Interv. 3 (1) (2010) 68–75.
[59] A. Tan, D. Goh, Y. Farhatnia, N. G, J. Lim, S.H. Teoh, J. Rajadas, M.S. Alavijeh, A. M. Seifalian, An anti-CD34 antibody-functionalized clinical-grade POSS-PCU nanocomposite polymer for cardiovascular stent coating applications: a preliminary assessment of endothelial progenitor cell capture and hemocompatibility, PLoS One 8 (10) (2013), e77112.
[60] J.I. Rotmans, J.M. Heyligers, H.J. Verhagen, E. Velema, M.M. Nagtegaal, D.P. de Kleijn, F.G. de Groot, E.S. Stroes, G. Pasterkamp, In vivo cell seeding with anti-CD34 antibodies successfully accelerates endothelialization but stimulates intimal hyperplasia in porcine arteriovenous expanded polytetrafluoroethylene grafts, Circulation 112 (1) (2005) 12–18.
[61] D. Wang, Y. Xu, Y.J. Lin, G. Yilmaz, J. Zhang, G. Schmidt, Q. Li, J.A. Thomson, L. S. Turng, Biologically functionalized expanded polytetrafluoroethylene blood vessel grafts, Biomacromolecules 21 (9) (2020) 3807–3816.
[62] J.M. Bastijanic, R.E. Marchant, F. Kligman, M.T. Allemang, R.O. Lakin, D. Kendrick, V.S. Kashyap, K. Kottke-Marchant, In vivo evaluation of biomimetic fluorosurfactant polymer-coated expanded polytetrafluoroethylene vascular grafts in a porcine carotid artery bypass model, J. Vasc. Surg. 63 (6) (2016) 1620–1630.
[63] Y. Liu, M.C. Munisso, A. Mahara, Y. Kambe, T. Yamaoka, Anti-platelet adhesion and in situ capture of circulating endothelial progenitor cells on ePTFE surface modified with poly(2-methacryloyloxyethyl phosphorylcholine) (PMPC) and hemocompatible peptide 1 (HCP-1), Colloids Surf. B Biointerfaces 193 (2020), 111113.
[64] M. Ferrell, V. Fuster, H.K. Gold, J.H. Chesebro, A dilemma for the 1990s. Choosing appropriate experimental animal model for the prevention of restenosis, Circulation 85 (4) (1992) 1630–1631.
[65] G.J. Johnson, T.R. Griggs, L. Badimon, The utility of animal models in the preclinical study of interventions to prevent human coronary artery restenosis: analysis and recommendations. On behalf of the Subcommittee on Animal, Cellular and Molecular Models of Thrombosis and Haemostasis of the Scientific and Standardization Committee of the International Society on Thrombosis and Haemostasis, Thromb. Haemostasis 81 (5) (1999) 835–843.
[66] B.S. Kelly, S.C. Heffelfinger, J.F. Whiting, M.A. Miller, A. Reaves, J. Armstrong, A. Narayana, P. Roy-Chaudhury, Aggressive venous neointimal hyperplasia in a pig model of arteriovenous graft stenosis, Kidney Int. 62 (6) (2002) 2272–2280.
[67] M. Narayanaswamy, K.C. Wright, K. Kandarpa, Animal models for atherosclerosis, restenosis, and endovascular graft research, J. Vasc. Intervent. Radiol. 11 (1) (2000) 5–17.
[68] R.O. Hynes, Cell-matrix adhesion in vascular development, J. Thromb. Haemostasis 5 (Suppl 1) (2007) 32–40.
[69] X. Cong, W. Kong, Endothelial tight junctions and their regulatory signaling pathways in vascular homeostasis and disease, Cell. Signal. 66 (2020), 109485.